Optical and Electrochemical Applications of Silicon–Carbon Dots/Silicon Dioxide Nanocomposites

Chung-Chien Shih,[†] Po-Cheng Chen,[†] Guan-Lin Lin, Chia-Wei Wang, and Huan-Tsung Chang*

Department of Chemistry, National Taiwan University, 1, Section 4, Roosevelt Road, Taipei 10617, Taiwan. [†]These authors contributed equally.

ABSTRACT Various colors of photoluminescent SiC-dots/SiO_2 prepared through a simple heating process have been employed for optical and electrochemical applications. Blue (B)-, green (G)-, and tan (T)-SiC-dots/SiO_2 powders have been prepared from SiC-dots that had been prepared from 3-aminopropyl trimethoxysilane through a hydrothermal route by simply controlling heating at 60 °C for 60 min and 300 °C for 10 and 20 min, respectively. The B-, G-, and T-SiC-dots/SiO_2 nanocomposites emit at 455, 534, and 574 nm, respectively, under excitation at 360 nm. B-, G-, and T-SiC-dots/SiO_2 glass films show at least seven colors when excited at 360, 460, and 520 nm. Through a heat-induced photoluminescence (PL) change, a representative lithographic pattern of B-SiC-dots/SiO_2 films has been fabricated using a near-infrared laser. The B-, G-, and T-SiC-dots/SiO_2 also possess high electrocatalytic activity for the oxygen reduction reaction. Having such interesting PL and electrical properties, the stable, low-toxic, and cost-effective B-, G-, and T-SiC-dots/SiO_2 nanocomposites show great economic potential in many applications such as light-emitting diodes, photoluminescent windows, and fuel cells.

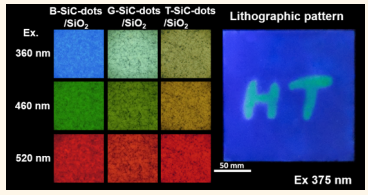

KEYWORDS: SiC-dots/SiO_2 nanocomposites · photoluminescent carbon dots · lithographic patterns · fuel cells · colorful glasses

Carbon nanodots (C-dots) possessing interesting optical, electrical, and catalytic properties have become attractive materials in sensing and catalysis.[1−5] C-dots show strong excitation wavelength dependent photoluminescence (PL).[5−10] Upon increasing excitation wavelength, the emission wavelength of C-dots undergoes a red shift, along with decreased emission intensity. Most C-dots emit at the wavelengths centered at 420−450 nm. The interesting optical properties of C-dots have been suggested to be correlated to their sizes and surface properties such as the presence of various types of chromophores with different degrees of double-bond conjugation and strain energies.[11−13] The emission of C-dots undergoes red shifts as their size increases.[14,15] The PL properties of C-dots can also be controlled through chemical modification of their surface functional groups (carbonyl, epoxy, and hydroxyl groups) to suppress their defect state emission.[16] Alternatively, doping of C-dots with elements such as nitrogen and sulfur in their lattice induces modulation of the chemical and electronic characteristics of the C-dots, leading to increased PL intensity and blue shifts in the emission wavelength.[17,18] To avoid incorporation of heteroatoms in the C-dot lattice to disrupt sp^2 hybridization of carbon atoms, tailoring the C-dots edge with ammonia or PEG-diamine has been demonstrated.[19,20]

C-dots have been prepared from various precursors, including ground coffee,[21] tea,[22] and small molecules such as glycine[15] and 3-aminopropyl trimethoxysilane (APTMS),[23] through simple hydrothermal routes. It has been suggested that precursors having carboxylate and amino groups are ideal for the preparation of hydrophilic C-dots with strong PL intensity. On the other hand, APTMS is ideal for the preparation of organosilane-functionalized C-dots (SiC-dots) that can be easily coated onto glass substrates through Si−O−Si bonding.[23]

C-dots have become popular sensing and imaging materials, but their use in fabrication of optical and electrical devices has not been well-recognized. Herein, a simple strategy for the preparation of various colors (emission wavelengths from 455 to 574 nm under excitation at 360 nm) of photoluminescent SiC-dots/SiO_2 nanocomposites was proposed. By simply varying the reaction temperature from 300 to 500 °C for 2 to 10 min or controlling the reaction time

* Address correspondence to changht@ntu.edu.tw.

Received for review August 26, 2014 and accepted December 18, 2014.

Published online December 18, 2014
10.1021/nn504787y

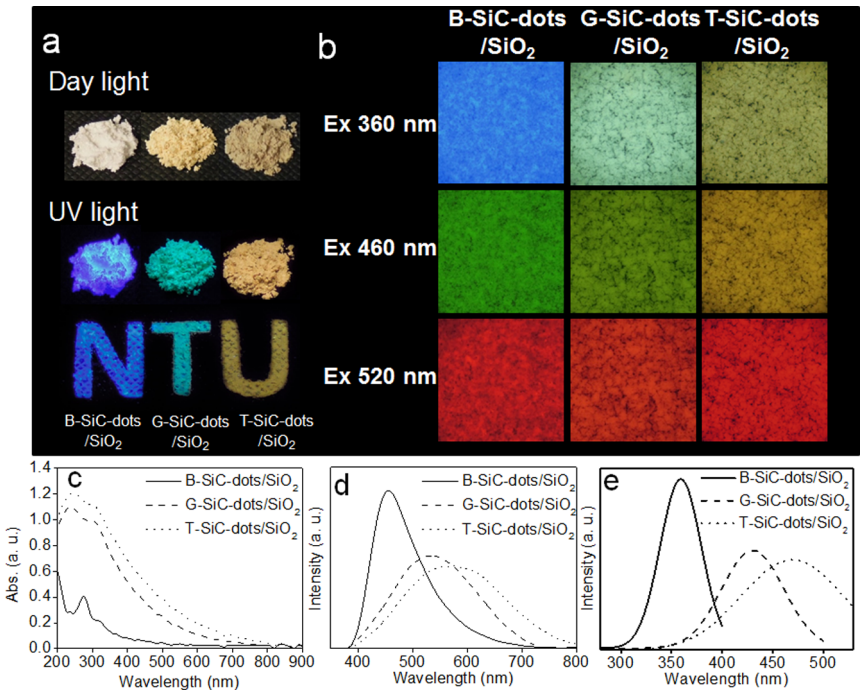

Figure 1. (a) Photographs of B-, G-, and T-SiC-dots/SiO_2 nanocomposite powders under irradiation of daylight (top) and UV light (middle). The bottom PL image of B-, G-, and T-SiC-dots/SiO_2 nanocomposite powders shows an abbreviation of our university. Excitation wavelength: 375 nm. (b) PL images of B-, G-, and T-SiC-dots/SiO_2 nanocomposite films excited at different wavelengths. (c–e) UV–vis absorption, emission, and excitation spectra of B-, G-, and T-SiC-dots/SiO_2 nanocomposite powders, respectively. The emission spectra were measured under excitation at 360 nm, and the excitation spectra were recorded at the emission wavelengths of 455, 534, and 574 nm for B-, G-, and T-SiC-dots/SiO_2 nanocomposite powders, respectively. PL intensities and absorbance are plotted in arbitrary units (au).

between 10 and 20 min at 300 °C, different colors of SiC-dots/SiO_2 nanocomposites were prepared. The PL properties of SiC-dots/SiO_2 nanocomposites are highly dependent on their morphologies, structures, and composition. As-prepared SiC-dots/SiO_2 nanocomposites can be easily coated onto plastic and glass substrates, with various colors and remarkable stability. For the first time, lithographic patterns of SiC-dots/SiO_2 nanocomposite films were fabricated using a near-infrared (NIR) laser with assistance of heating. As-prepared SiC-dots/SiO_2 nanocomposites also possess electrocatalytic activity for the oxygen reduction reaction (ORR) in an alkaline medium. This study opens up a great avenue of SiC-dots/SiO_2 nanocomposites for the fabrication of optical and electrical devices.

RESULTS AND DISCUSSION

Optical Properties of SiC-Dots/SiO_2 Nanocomposites. Under UV irradiation, the SiC-dots/SiO_2 nanocomposite powders prepared at 60 °C for 60 min and 300 °C for 10 and 20 min emitted blue, green, and tan colors. It is important to note that most of reported C-dots only have strong PL in the blue region under UV irradiation.[20] The emission shift is dependent on temperature and heating time, as shown in Figure S1 (Supporting Information). B-SiC-dots/SiO_2 nanocomposites were dried at 60 °C without changing their optical properties. The degree of emission shift increased upon increasing heating temperature over 100–300 °C for a certain heating time. It took a longer time for the same shift at lower temperature. At 300, 400, and 500 °C, it separately took 10, 5, and 2 min to convert blue (B)-SiC-dots/SiO_2 to tan (T)-SiC-dots/SiO_2 nanocomposites. However, at higher temperature (>300 °C), the size distribution of SiC-dots/SiO_2 nanocomposites becomes wider and inhomogeneous. Therefore, green (G)- and T-SiC-dots/SiO_2 nanocomposites were prepared at 300 °C for further study. The as-prepared B-, G-, and T-SiC-dots/SiO_2 nanocomposite powders were used to pattern the abbreviation NTU of our university, as shown in Figure 1a. They were further used to prepare three films (Figure 1b) showing interesting excitation wavelength dependent PL characteristics like that of reported C-dots.[5–9] While the exact PL mechanism of C-dots still remains unsolved, several plausible mechanisms have been proposed such as recombination of electron/hole pairs of carbon, surface energy traps/states (some defects on the surface of C-dots), and quantum confinement effect.[10–12,16,24] Using the three different colors of SiC-dots/SiO_2 nanocomposites, at least seven different colors of PL images were generated when excited at three different wavelengths, revealing their potential use as multicolor inks and for the fabrication of colorful glasses. The SiC-dots/SiO_2 nanocomposite powders and films were all quite stable in air under daylight irradiation for at least

12 months. Relative to most C-dots, the SiC-dots/SiO_2 nanocomposite powders and films are more stable against photoirradiation, mainly because of adsorption of SiC-dots on SiO_2 nanoparticles (white aggregates), minimizing aggregation of SiC-dots.[25] The SiO_2 nanoparticles were formed through the hydrolysis of the excess APTMS according to the Stöber method.[26] Figure 1c displays that B-SiC-dots/SiO_2 nanocomposites have a distinct absorption at 275 nm, which is attributed to the $\pi-\pi^*$ transitions of the sp^2 domain.[23] The absorption edge shifts to longer wavelengths for G- and T-SiC-dots/SiO_2 nanocomposites, implying that the sizes of G- and T-SiC-dots/SiO_2 nanocomposites are larger than that of B-SiC-dots/SiO_2 nanocomposites.[27]

Figure 1d displays that the B-, G-, and T-SiC dots/SiO_2 nanocomposites emit at 455, 534, and 574 nm, respectively, under excitation at 360 nm, with full widths at half-maximum (fwhm) values of 103, 179, and 217 nm, respectively. To the best of our knowledge, such strong green and tan PL colors of C-dots have not been reported. Increases in the fwhm are likely due to increases in the size variation of SiC-dots adsorbed on SiO_2 nanoparticles.[28] The PL intensity of B-SiC-dots/SiO_2 nanocomposites at 455 nm is about 1.7- and 1.9-fold stronger than that of the G- and T-SiC-dots/SiO_2 nanocomposites at 534 and 574 nm, respectively. This is in good agreement with the blue PL of C-dots being stronger than their red PL.[5,10,29] The B-, G-, and T-SiC-dots/SiO_2 nanocomposites have excitation spectral profiles similar to their corresponding emission profiles (Figure 1e), with maximum excitation wavelengths at 360, 430, and 480 nm, respectively. The presence of a broader absorption band and a tail for G- or T-SiC-dots/SiO_2 nanocomposites indicates the existence of defect states, which is similar to C-dots containing many oxygen functional groups.[14,30] The quantum yields of B-, G-, and T-SiC-dots/SiO_2 nanocomposite powders are 6.7, 0.6, and 0.1%, respectively, and their films have quantum yields of 0.7, 0.8, and 0.1%, respectively.

To study the recombination dynamics of B-, G-, and T-SiC-dots/SiO_2 nanocomposites, their time-resolved PL decay curves were recorded at 455, 534, and 574 nm, respectively, with an excitation wavelength at 375 nm. They all show biexponential decay curves with fast and slow decay components.[14,30,31] Their average lifetime (τ_{av}) values were calculated by using $\tau_{av} = (A_1\tau_1 + A_2\tau_2)/(A_1 + A_2)$, in which A_1 and A_2 are the amplitudes of the two lifetime components. The average lifetimes for B-, G-, and T-SiC-dots/SiO_2 nanocomposites are 7.7 $\pm$ 0.1 ns (A_1 = 60%; A_2 = 40%), 5.4 $\pm$ 0.1 ns (A_1 = 67%; A_2 = 23%), and 2.4 $\pm$ 0.08 ns (A_1 = 74%; A_2 = 26%), respectively. The G- and T-SiC-dots/SiO_2 nanocomposites have shorter lifetimes and weaker PL intensities than those of B-SiC-dots/SiO_2 nanocomposites, mainly due to increased surface defects after thermal treatment.

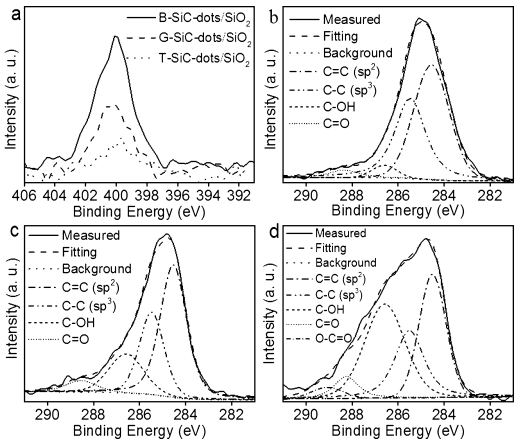

Figure 2. XPS spectra of (a) N 1s and (b–d) C 1s of B-, G-, and T-SiC-dots/SiO_2 nanocomposites. C 1s spectra of (b) B-, (c) G-, and (d) T-SiC-dots/SiO_2 nanocomposites. The deconvoluted peaks correspond to sp^2 (C=C) at 284.5 eV, sp^3 (C–C and C–H) at 285.5 eV, C–OH at 286.6 eV, C–O–C at 287.2 eV, and C=O at 288.6 eV.

Characteristics of SiC-Dots/SiO_2 Nanocomposites. Fourier transform infrared (FTIR) spectra of the B-, G-, and T-SiC-dots/SiO_2 nanocomposites (Figure S2, Supporting Information) all show characteristic absorption bands for N–H and O–H stretching vibrations of the amino and hydroxyl groups near 3100 and 3300 cm^{-1}, supporting their hydrophilicity. Two signals at 1010 and 1090 cm^{-1} are for Si–O–Si and Si–O–C vibrations, respectively, confirming the presence of Si atoms in each sample. Unlike that in B-SiC-dots/SiO_2 nanocomposites, either G- or T-SiC-dots/SiO_2 nanocomposites do not have peaks for N–H stretching and bending vibrations at 3100 and 1550 cm^{-1}. An absorption band due to C=O stretching vibration at 1630 cm^{-1} was found in T-SiC-dots/SiO_2 nanocomposites, indicating that oxidation occurred during heating. The data suggested the decrease of nitrogen content in the G- and T-SiC-dots/SiO_2 compared to that in the B-SiC-dots/SiO_2 nanocomposites. The energy-dispersive X-ray spectroscopy data confirm that the three types of SiC-dots/SiO_2 nanocomposites all contain carbon, nitrogen, oxygen, and silicon (Figure S3, Supporting Information). The contents of Si in the three types of SiC-dots/SiO_2 nanocomposites increase in the order of B < G < T, revealing that more SiO_2 nanoparticles were formed when heating was conducted at higher temperature for a longer time.[32] The elemental analysis data (Table S1, Supporting Information) and X-ray photoelectron spectroscopy (XPS) data (Figure 2) display that, relative to B-SiC-dots/SiO_2 nanocomposites, G- and T-SiC-dots/SiO_2 nanocomposites have less carbon and nitrogen content, revealing that oxidation occurred during heating. The decreased nitrogen contents revealed that some nitrogen atoms were released from SiC-dots to leave some vacancies (defects).[14] The trend of oxygen contents of SiC-dots/SiO_2 nanocomposites decreases in the order

of B < T < G, supporting the formation of SiO_2 nanoparticles and oxidation. The XPS data support the changes in the compositions of SiC-dots/SiO_2 nanocomposites during heating. The peaks assigned for N consisting of both pyridine-like (398.5 eV) and pyrrole (401 eV) show significant differences among the three SiC-dots/SiO_2 nanocomposites.[17] The high-resolution C 1s spectrum of the B-SiC-dots/SiO_2 nanocomposites at 284.5 eV confirms their graphitic structure (sp^2 C═C).[33] The peak at 286.6 eV reveals the formation of more C−OH groups on G-SiC-dots/SiO_2 nanocomposites, supporting the occurrence of oxidation during heating. The C 1s peak for T-SiC-dots/SiO_2 nanocomposites is much broader when compared to that of B- and G-SiC-dots/SiO_2 nanocomposites, mainly because of the presence of O−C−O (287.2 eV) and C═O (288.6 eV). The XPS spectra of Si $2p_{3/2}$ depicted in Figure S4 (Supporting Information) confirm the presence of Si−O bonding. The binding energies for Si $2p_{3/2}$ in the G- and T-SiC-dots/SiO_2 nanocomposites are both 0.8 eV higher than that of B-SiC-dots/SiO_2 nanocomposites, revealing their increased O−Si−O bond and decreased C−Si−O bond.[34] The decrease of C−Si−O is in good agreement with the reduction of carbon determined by the elemental analysis.

The peak ratios (I_D/I_G) for B-, G-, and T-SiC-dots/SiO_2 nanocomposites were estimated from their corresponding Raman spectra (Figure S5, Supporting Information) to be 0.93, 0.86, and 0.74, respectively, in which the peak (G) at ~1600 cm^{-1} corresponds to the E_{2g} mode of graphite and the peak (D) at ~1370 cm^{-1} is correlated with the breathing modes of six-atom rings.[20,35] The results suggest that removal of nitrogen caused the loss of sp^2 rings (increase defects), leading to the decreased D band signal.[35]

The TEM images (Figure S6, Supporting Information) of B-, G-, and T-SiC-dots/SiO_2 nanocomposites display that the aggregation of SiC-dots/SiO_2 nanocomposites increases in the order of B < G < T, revealing that heat induced their aggregation (Figure 3). The size distribution of SiC-dots in B-, G-, and T-SiC-dots/SiO_2 nanocomposites (100 counts) is 6.0 ± 0.5, 15 ± 1.5, and 18 ± 1 nm, respectively. The sizes of these SiC-dots are close to that reported in the literature.[27,36] The emission band of SiC-dots/SiO_2 nanocomposites is red-shifted upon increasing the size of SiC-dots.[27,37] The size distribution of SiC-dots in B-SiC-dots/SiO_2 nanocomposites is significantly smaller than that of G- and T-SiC-dots/SiO_2 nanocomposites, leading to a sharper emission band of B-SiC-dots/SiO_2 nanocomposites.

Role of SiO_2 Nanoparticles. To understand the role that SiO_2 nanoparticles played in determining the optical properties of SiC-dots/SiO_2 nanocomposites, a HF aqueous solution (1%) was used to dissolve the SiO_2 nanoparticles. After being treated with HF, the milky white background due to SiO_2 nanoparticles in the B-, G-, and T-SiC-dots/SiO_2 nanocomposite solutions all disappeared (Figure 4a,b). Figure 4c shows that the PL of B-SiC-dots/SiO_2 nanocomposites only slightly changes after etching, revealing that SiC-dots are highly stable under such a harsh condition. However, the PL wavelengths for G- and T-SiC-dots/SiO_2 nanocomposites significantly undergo blue shifts to 440 nm after etching, while each with a shoulder in the long-wavelength region (>500 nm), which is in good agreement with the presence of larger SiC-dots in G- and T-SiC-dots/SiO_2 nanocomposites. This result implies that the presence of SiO_2 nanoparticles is essential for the red shift of PL. The emitted light from the smaller SiC-dots traveling through SiO_2 nanoparticles was reabsorbed by large SiC-dots, leading to a red shift.[38] In addition, the PL of G- and T-SiC-dots/SiO_2 nanocomposites almost does not change after being treated with HCl or HNO_3 at the

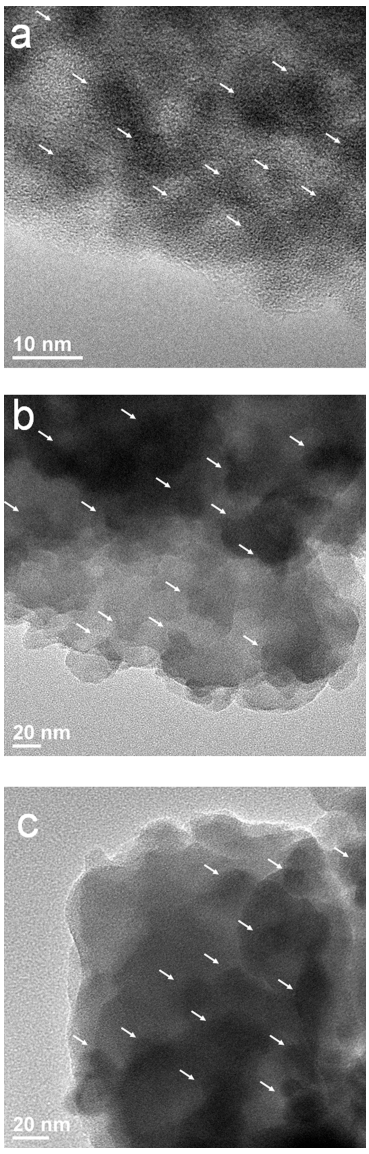

Figure 3. HRTEM images of as-prepared (a) B-, (b) G- and (c) T-SiC-dots/SiO_2 nanocomposites. The white arrows indicate the location of SiC-dots.

concentrations up to 10%. The result reveals that the heating-induced PL shifts of SiC-dots/SiO_2 nanocomposites are mainly due to the formation of SiO_2 nanoparticles. In addition, increases in the size and oxidation degree of SiC-dots and reduced amounts of the nitrogen groups during heating are also responsible for the changes in the PL properties of SiC-dots/SiO_2 nanocomposites.[16,17,30,39]

Applications of SiC-Dots/SiO_2 Nanocomposites. Figure 5a displays the cyclic voltammograms (CVs) of B-, G-, and T-SiC-dots/SiO_2 nanocomposites in O_2-saturated KOH solutions, each with a well-defined cathodic peak at −0.43 V. As a control, an electrode fabricated with SiC-dots without being subjected to heating was used. The ORR onset potential of each electrode was found to be at *ca.* −0.26 V. The reduction current densities at −0.43 V for B-, G-, and T-SiC-dots/SiO_2 nanocomposite electrodes are 0.43, 0.40, and 0.37 mA cm^{-2}, respectively; the decreased order agrees with that of their nitrogen content. Nitrogen groups facilitate the electron transfer from carbon electronic bands to an antibonding orbital of O_2, enhancing their ORR activity.[40,41] All of the four electrodes exhibit stable ORR activity in the methanol-containing electrolyte (Figure 5b), showing no electroactivity specific to methanol. The result reveals their remarkable tolerance to possible crossover effects. Unlike how the signal decreased significantly (about 32%) in the control electrode after 200 cycles, their catalytic activities remained almost constant (<3%) even after at least 500 cycles for the other three electrodes. The loss of activity of the control electrode is mainly due to the loss of SiC-dots/SiO_2 nanocomposites from the electrode. The remarkable stability of the three electrodes was also supported by no changes in their PL images after being soaked with 0.5 M KOH for 1 day (Figure 5c). The results demonstrated great practicality of the electrodes for direct methanol fuel cells.

The B-, G-, and T-SiC-dots/SiO_2 nanocomposites were used to prepare a homogeneous coating of glass and plastic substrates (not shown), showing features of simplicity, homogeneity, and great stability. The results encouraged us to do lithographic patterns on SiC-dot/SiO_2 films. Since it is easier to tune the PL color from B-SiC-dots/SiO_2 nanocomposites than from the other two, B-SiC-dots/SiO_2 nanocomposite films were subjected to laser irradiation. Under irradiation of NIR light for 10 min during heating, a representative pattern with HT was obtained in the film, as shown in Figure 6. The pattern fabricated 12 months ago still remains stable in the ambient environment. Our preliminary result suggests that B-SiC-dots/SiO_2 nanocomposites hold great potential for luminescence pattern printing and for fabrication of optical devices.

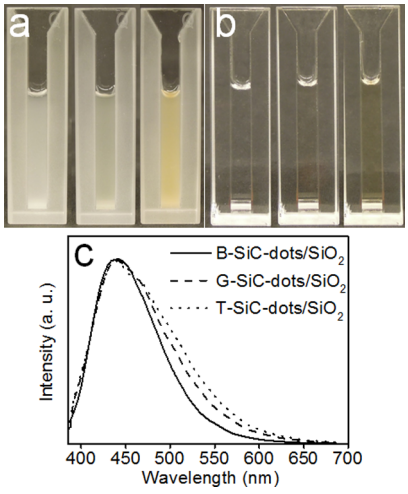

Figure 4. B-, G-, and T-SiC-dots/SiO_2 solutions (a) before and (b) after being etched with 1% HF. Left, middle, and right cells in (a) and (b) were filled with B-, G-, and T-SiC-dots/SiO_2 nanocomposite solutions, respectively. (c) PL spectra of B-, G-, and T-SiC-dots/SiO_2 solutions after HF etching, which are plotted in arbitrary units (au). Their actual PL intensity ratio is 1.4:1.1:1.0 of T-SiC-dots/SiO_2 solutions. Excitation wavelength: 360 nm.

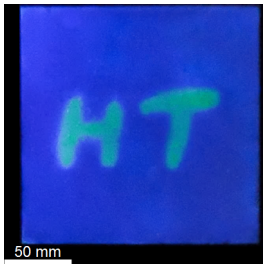

Figure 6. Representative lithographic pattern (HT) of B-SiC-dots/SiO_2 nanocomposite films (1.8 × 1.8 cm). NIR laser was used for patterning. UV light source at 375 nm was used to excite the film to induce PL.

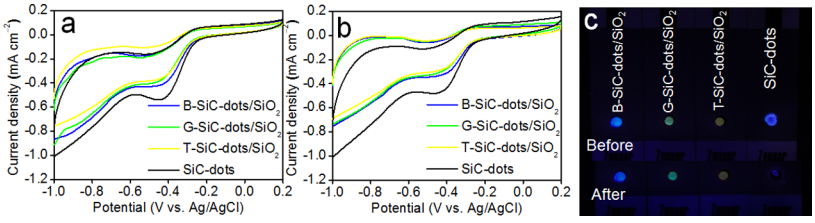

Figure 5. CVs (a,b) and PL images (c) of SiC-dots, B-, G-, and T-SiC-dots/SiO_2 nanocomposite modified electrodes. Electrolytes: O_2-saturated 0.5 M KOH solutions (a) without and (b) with 0.5 M CH_3OH. (c) PL image of the SiC-dot modified electrode was taken after 200 cycles of CV measurements in O_2-saturated 0.5 M KOH solution containing 0.5 M CH_3OH, while the other three electrodes were taken after 500 cycles of CV measurements.

CONCLUSIONS

A simple heating approach was employed to prepare B-, G-, and T-SiC-dots/SiO_2 nanocomposite powders and films from SiC-dots. The heat-induced PL shift is attributed to a combination of several factors, including the formation of SiC-dots/SiO_2 nanocomposites, change in sizes, and composition of SiC-dots. The B-, G-, and T-SiC-dots/SiO_2 powders and films are extremely stable, showing their possible use as fluorescent inks and for fabrication of colorful glasses. SiC-dots/SiO_2 nanocomposites with advantages of stability and electrocatalytic activity toward ORR are useful catalysts for fuel cells. Lithographic patterns of B-SiC-dots/SiO_2 nanocomposite films further show their use in fabrication of microscale devices.

METHODS

Chemicals. Methanol, ethanol, APTMS, hydrogen fluoride (HF), Nafion, and sulfuric acid were purchased from Sigma-Aldrich (Milwaukee, WI). Potassium hydroxide (KOH) was purchased from Merck (Whitehouse Station, NJ). Piranha solution was prepared by mixing 3:1 volumes of concentrated sulfuric acid with 30% hydrogen peroxide solution (Showa, Tokyo, Japan). Ultrapure water (18.2 MΩ·cm) was obtained from a Milli-Q ultrapure system (Billerica, MA).

Synthesis of Various Colors of SiC-Dots/SiO_2 Nanocomposite Powders. SiC-dots were prepared from APTMS through a hydrothermal route.[23] A Nabertherm LT 40/12 (Lilienthal, Germany) furnace was used in the hydrothermal synthesis and calcination. Through condensation of excess APTMS, white precipitates containing SiC-dots and SiO_2 nanoparticles were formed from the as-prepared SiC-dots. The white precipitates were subjected to two cycles of centrifugation (centrifugation force 3000*g*)/wash (15 mL × 2) and then dried in an oven at 60 °C for 60 min to form a white powder. This white powder emitted blue color and thus is represented as blue SiC-dots/SiO_2 (B-SiC-dots/SiO_2) nanocomposites. By conducting similar processes, but with calcination of the powers at 300 °C for 10 and 20 min under ambient pressure, green and tan SiC-dots/SiO_2 (G-SiC-dots/SiO_2 and T-SiC-dots/SiO_2) nanocomposites were prepared, respectively. The powders were also subjected to calcination at 400 and 500 °C for 5 and 2 min to support the heating effect on the change in the optical properties of SiC-dots/SiO_2 nanocomposites.

Preparation of B-, G-, and T-SiC-Dots/SiO_2 Nanocomposite Films. Prior to use for the preparation of SiC-dots/SiO_2 nanocomposite films, glass substrates were thoroughly rinsed with ultrapure water and dried in an oven at 60 °C for 30 min. The glass substrates were then treated with piranha solution for 15 min, followed by washing with water (50 mL) and ethanol (50 mL) for 15 min each. The clean substrates were immersed in SiC-dots aqueous solution overnight. They were then taken out and subjected to heating at 60 °C for 60 min to prepare B-SiC-dots/SiO_2 nanocomposite films and at 300 °C for 10 and 20 min to prepare G-SiC-dots/SiO_2 and T-SiC-dots/SiO_2 nanocomposite films, respectively.

Characterization of B-, G-, and T-SiC-Dots/SiO_2 Nanocomposites. PL spectra of B-, G-, and T-SiC-dots/SiO_2 nanocomposite films were measured by using an Olympus IX71 (Tokyo, Japan) fluorescence microscope with Acton SP2150 monochromator and ProEM 512B EMCCD both from Princeton Instruments (Trenton, NJ). PL images of SiC-dots/SiO_2 nanocomposite films were measured by using an Olympus IX71 fluorescence microscope with a digital camera from Nikon P300 (Tokyo, Japan). Owing to the limit of the microscopic system, the excitation wavelengths were set in three different ranges of 510−530, 460−480, and 360−380 nm. Excitation spectra were taken using a HORIBA FluoroMax-3 spectrometer (Kyoto, Japan). Quantum yields of B-, G-, and T-SiC-dots/SiO_2 nanocomposites were determined using an absolute PL quantum yield spectrometer (Quantaurus-QY, Hamamatsu Photonics K.K., Hamamatsu, Japan). PL lifetimes were recorded using an Timp Harp 200 time-correlated single photon counting system (PicoQuant, Berlin, Germany), equipped with a 375 nm laser (LDH-P-C-375, PicoQuant, Berlin, Germany) as an excitation source. A 380 nm long-pass, 405/150 nm band-pass, and 580/60 nm band-pass filters were separately used to minimize scattering light. Prior to conducting transmission electron microscopy (TEM) and high-resolution TEM (HRTEM) measurements, the as-prepared B-, G-, and T-SiC-dots/SiO_2 nanocomposites were diluted with water (0.5 mg mL^{-1}). Each of the SiC-dots/SiO_2 nanocomposite solutions was carefully deposited on a 400-mesh C-coated Cu grid, and the excess solvent was evaporated at ambient temperature (25 °C) and pressure. To record the size and shape of the as-prepared SiC-dots/SiO_2 nanocomposites, JSM-1200EX II (JEOL Ltd., Tokyo, Japan) and FEI Tecnai-G2-F20 TEMs were used. The compositions of the SiC-dots/SiO_2 nanocomposites were determined by conducting elemental analyses (Vario EL-III, GmbH, Hanau, Germany) and energy-dispersive X-ray spectroscopy (Philips, Roanoke, VA, USA). A Varian 640 FTIR spectrophotometer (Varian, USA) was used to analyze the as-prepared B-, G-, and T-SiC-dots/SiO_2 nanocomposites. X-ray photoelectron spectroscopy was performed using a VG ESCA210 electron spectroscope from VG Scientific (West Sussex, UK). A Raman microscopy system with a 50× objective (Dongwoo Optron, KyungGiDo, Korea) was used to analyze air-dried B-, G-, and T-SiC-dots/SiO_2 nanocomposites on silica wafers.

Electrocatalysis. Aliquots (5 μL) of the as-synthesized B-, G-, and T-SiC-dots/SiO_2 nanocomposite solutions (1 mg/mL) were separately dropped onto clean screen-printed electrodes (No. SE101-GK, Zensor R&D, Taichung, Taiwan; diameter: 3 mm). After the electrodes were air-dried at ambient temperature for 1 h, Nafion solution (0.5%, 1 μL) was placed onto each of the electrodes. Three-electrode electrochemical cells were fabricated using the modified electrode as a working electrode, a Pt wire as an auxiliary electrode, and a Ag/AgCl electrode as a reference electrode. The electrocatalytic activities of the as-synthesized B-, G-, and T-SiC-dots/SiO_2 nanocomposites were measured using a CHI 760D electrochemical workstation (Austin, TX). Cyclic voltammetry measurements in 0.5 M KOH with or without 0.5 M methanol under oxygen purge were conducted over the potential range from −1.0 to 0.2 V at a scan rate of 100 mV s^{-1}.

Lithography of B-SiC-Dots/SiO_2 Nanocomposite Films. Lithography of B-SiC-dots/SiO_2 nanocomposite films was carried out by using a NIR laser (Power Technology, Little Rock, AR) with emission at 808 nm. B-SiC-dots/SiO_2 nanocomposite films were first heated on a hot plate to 250 °C. The NIR laser was placed on top of the film (about 15 cm from the film). By moving the laser light, lithographic patterns of B-SiC-dots/SiO_2 nanocomposite films were achieved.

Conflict of Interest: The authors declare no competing financial interest.

Acknowledgment. This study was supported by the Ministry of Science and Technology under Contract 101-2113-M-002-002-MY3. The assistance of Ya-Yu Yang from the Instrument Center of National Taiwan University (NTU) for TEM measurement is appreciated.

Supporting Information Available: Compositions of B-, G-, and T-SiC-dots/SiO_2 nanocomposites determined by elemental analysis. PL spectra of SiC-dots/SiO_2 nanocomposites heated at different temperatures for various times; FTIR spectra of SiC-dots/SiO_2 nanocomposites; EDS spectra of SiC-dots/SiO_2 nanocomposites; XPS spectra of Si 2p of SiC-dots/SiO_2 nanocomposites; normalized Raman spectra of SiC-dots/SiO_2

nanocomposites and TEM images of SiC-dots/SiO_2 nanocomposites. This material is available free of charge *via* the Internet at http://pubs.acs.org.

REFERENCES AND NOTES

1. Ritter, K. A.; Lyding, J. W. The Influence of Edge Structure on the Electronic Properties of Graphene Quantum Dots and Nanoribbons. *Nat. Mater.* **2009**, *8*, 235–242.
2. Zhang, Z.; Zhang, J.; Chen, N.; Qu, L. Graphene Quantum Dots: An Emerging Material for Energy-Related Applications and Beyond. *Energy Environ. Sci.* **2012**, *5*, 8869–8890.
3. Zhou, J.; Booker, C.; Li, R.; Zhou, X.; Sham, T.-K.; Sun, X.; Ding, Z. An Electrochemical Avenue to Blue Luminescent Nanocrystals from Multiwalled Carbon Nanotubes (MWCNTs). *J. Am. Chem. Soc.* **2007**, *129*, 744–745.
4. Zhou, L.; Lin, Y.; Huang, Z.; Ren, J.; Qu, X. Carbon Nanodots as Fluorescence Probes for Rapid, Sensitive, and Label-Free Detection of Hg^{2+} and Biothiols in Complex Matrices. *Chem. Commun.* **2012**, *48*, 1147–1149.
5. Baker, S. N.; Baker, G. A. Luminescent Carbon Nanodots: Emergent Nanolights. *Angew. Chem., Int. Ed.* **2010**, *49*, 6726–6744.
6. Wang, X.; Qu, K.; Xu, B.; Ren, J.; Qu, X. Microwave Assisted One-Step Green Synthesis of Cell-Permeable Multicolor Photoluminescent Carbon Dots without Surface Passivation Reagents. *J. Mater. Chem.* **2011**, *21*, 2445–2450.
7. Li, H.; Kang, Z.; Liu, Y.; Lee, S.-T. Carbon Nanodots: Synthesis, Properties and Applications. *J. Mater. Chem.* **2012**, *22*, 24230–24253.
8. Li, L.; Wu, G.; Yang, G.; Peng, J.; Zhao, J.; Zhu, J. J. Focusing on Luminescent Graphene Quantum Dots: Current Status and Future Perspectives. *Nanoscale* **2013**, *5*, 4015–4039.
9. Shen, J.; Zhu, Y.; Yang, X.; Li, C. Graphene Quantum Dots: Emergent Nanolights for Bioimaging, Sensors, Catalysis and Photovoltaic Devices. *Chem. Commun.* **2012**, *48*, 3686–3699.
10. Sun, Y. P.; Zhou, B.; Lin, Y.; Wang, W.; Fernando, K. A. S.; Pathak, P.; Meziani, M. J.; Harruff, B. A.; Wang, X.; Wang, H. F.; *et al.* Quantum-Sized Carbon Dots for Bright and Colorful Photoluminescence. *J. Am. Chem. Soc.* **2006**, *128*, 7756–7757.
11. Eda, G.; Lin, Y.-Y.; Mattevi, C.; Yamaguchi, H.; Chen, H.-A.; Chen, I. S.; Chen, C.-W.; Chhowalla, M. Blue Photoluminescence from Chemically Derived Graphene Oxide. *Adv. Mater.* **2010**, *22*, 505–509.
12. Pan, D. Y.; Zhang, J. C.; Li, Z.; Wu, M. H. Hydrothermal Route for Cutting Graphene Sheets into Blue-Luminescent Graphene Quantum Dots. *Adv. Mater.* **2010**, *22*, 734–738.
13. Bourlinos, A. B.; Zboril, R.; Petr, J.; Bakandritsos, A.; Krysmann, M.; Giannelis, E. P. Luminescent Surface Quaternized Carbon Dots. *Chem. Mater.* **2012**, *24*, 6–8.
14. Peng, J.; Gao, W.; Gupta, B. K.; Liu, Z.; Romero-Aburto, R.; Ge, L.; Song, L.; Alemany, L. B.; Zhan, X.; Gao, G.; *et al.* Graphene Quantum Dots Derived from Carbon Fibers. *Nano Lett.* **2012**, *12*, 844–849.
15. Hsu, P. C.; Chang, H. T. Synthesis of High-Quality Carbon Nanodots from Hydrophilic Compounds: Role of Functional Groups. *Chem. Commun.* **2012**, *48*, 3984–3986.
16. Zhu, S.; Zhang, J.; Tang, S.; Qiao, C.; Wang, L.; Wang, H.; Liu, X.; Li, B.; Li, Y.; Yu, W.; *et al.* Surface Chemistry Routes to Modulate the Photoluminescence of Graphene Quantum Dots: From Fluorescence Mechanism to Up-Conversion Bioimaging Applications. *Adv. Funct. Mater.* **2012**, *22*, 4732–4740.
17. Li, Y.; Zhao, Y.; Cheng, H.; Hu, Y.; Shi, G.; Dai, L.; Qu, L. Nitrogen-Doped Graphene Quantum Dots with Oxygen-Rich Functional Groups. *J. Am. Chem. Soc.* **2011**, *134*, 15–18.
18. Dong, Y.; Pang, H.; Yang, H. B.; Guo, C.; Shao, J.; Chi, Y.; Li, C. M.; Yu, T. Carbon-Based Dots Co-doped with Nitrogen and Sulfur for High Quantum Yield and Excitation-Independent Emission. *Angew. Chem., Int. Ed.* **2013**, *52*, 7800–7804.
19. Jin, S. H.; Kim, D. H.; Jun, G. H.; Hong, S. H.; Jeon, S. Tuning the Photoluminescence of Graphene Quantum Dots through the Charge Transfer Effect of Functional Groups. *ACS Nano* **2012**, *7*, 1239–1245.
20. Tetsuka, H.; Asahi, R.; Nagoya, A.; Okamoto, K.; Tajima, I.; Ohta, R.; Okamoto, A. Optically Tunable Amino-Functionalized Graphene Quantum Dots. *Adv. Mater.* **2012**, *24*, 5333–5338.
21. Hsu, P. C.; Shih, Z. Y.; Lee, C. H.; Chang, H. T. Synthesis and Analytical Applications of Photoluminescent Carbon Nanodots. *Green Chem.* **2012**, *14*, 917–920.
22. Hsu, P. C.; Chen, P. C.; Ou, C. M.; Chang, H. Y.; Chang, H. T. Extremely High Inhibition Activity of Photoluminescent Carbon Nanodots toward Cancer Cells. *J. Mater. Chem. B* **2013**, *1*, 1774–1781.
23. Chen, P. C.; Chen, Y. N.; Hsu, P. C.; Shih, C. C.; Chang, H. T. Photoluminescent Organosilane-Functionalized Carbon Dots as Temperature Probes. *Chem. Commun.* **2013**, *49*, 1639–1641.
24. Li, L. L.; Ji, J.; Fei, R.; Wang, C. Z.; Lu, Q.; Zhang, J. R.; Jiang, L. P.; Zhu, J. J. A Facile Microwave Avenue to Electrochemiluminescent Two-Color Graphene Quantum Dots. *Adv. Funct. Mater.* **2012**, *22*, 2971–2979.
25. Jung, H. S.; Kim, Y. J.; Ha, S. W.; Lee, J. K. White Light-Emitting Diodes Using Thermally and Photochemically Stable Fluorescent Silica Nanoparticles as Color-Converters. *J. Mater. Chem. C* **2013**, *1*, 5879–5884.
26. Stöber, W.; Fink, A.; Bohn, E. Controlled Growth of Monodisperse Silica Spheres in the Micron Size Range. *J. Colloid Interface Sci.* **1968**, *26*, 62–69.
27. Kim, S.; Hwang, S. W.; Kim, M.-K.; Shin, D. Y.; Shin, D. H.; Kim, C. O.; Yang, S. B.; Park, J. H.; Hwang, E.; Choi, S.; *et al.* Anomalous Behaviors of Visible Luminescence from Graphene Quantum Dots: Interplay between Size and Shape. *ACS Nano* **2012**, *6*, 8203–8208.
28. Maeda, Y. Visible Photoluminescence from Nanocrystallite Ge Embedded in a Glassy SiO_2 Matrix: Evidence in Support of the Quantum-Confinement Mechanism. *Phys. Rev. B* **1995**, *51*, 1658–1670.
29. Krysmann, M. J.; Kelarakis, A.; Dallas, P.; Giannelis, E. P. Formation Mechanism of Carbogenic Nanoparticles with Dual Photoluminescence Emission. *J. Am. Chem. Soc.* **2011**, *134*, 747–750.
30. Liu, F.; Jang, M. H.; Ha, H. D.; Kim, J. H.; Cho, Y. H.; Seo, T. S. Facile Synthetic Method for Pristine Graphene Quantum Dots and Graphene Oxide Quantum Dots: Origin of Blue and Green Luminescence. *Adv. Mater.* **2013**, *25*, 3657–3662.
31. Xie, Z.; Wang, F.; Liu, C. Y. Organic−Inorganic Hybrid Functional Carbon Dot Gel Glasses. *Adv. Mater.* **2012**, *24*, 1716–1721.
32. Grudzien, R. M.; Grabicka, B. E.; Jaroniec, M. Effective Method for Removal of Polymeric Template from SBA-16 Silica Combining Extraction and Temperature-Controlled Calcination. *J. Mater. Chem.* **2006**, *16*, 819–823.
33. Tang, L.; Ji, R.; Cao, X.; Lin, J.; Jiang, H.; Li, X.; Teng, K. S.; Luk, C. M.; Zeng, S.; Hao, J.; *et al.* Deep Ultraviolet Photoluminescence of Water-Soluble Self-Passivated Graphene Quantum Dots. *ACS Nano* **2012**, *6*, 5102–5110.
34. a) Jing, S. Y.; Lee, H. J.; Choi, C. K. Chemical Bond Structure on Si−O−C Composite Films with a Low Dielectric Constant Deposited by Using Inductively Coupled Plasma Chemical Vapor Deposition. *J. Korean Phys. Soc.* **2002**, *41*, 769–773. b) Fang, Y. X.; Guo, S. J.; Li, D.; Zhu, C. Z.; Ren, W.; Dong, S. J.; Wang, E. K. Easy Synthesis and Imaging Applications of Cross-Linked Green Fluorescent Hollow Carbon Nanoparticles. *ACS Nano* **2012**, *6*, 400–409.
35. Ferrari, A. C.; Basko, D. M. Raman Spectroscopy as a Versatile Tool for Studying the Properties of Graphene. *Nat. Nanotechnol.* **2013**, *8*, 235–246.
36. Xu, Q.; Zhou, Q.; Hua, Z.; Xue, Q.; Zhang, C.; Wang, X.; Pan, D.; Xiao, M. Single-Particle Spectroscopic Measurements of Fluorescent Graphene Quantum Dots. *ACS Nano* **2013**, *7*, 10654–10661.
37. Li, H.; He, X.; Kang, Z.; Huang, H.; Liu, Y.; Liu, J.; Lian, S.; Tsang, C. H. A.; Yang, X.; Lee, S.-T. Water-Soluble Fluorescent Carbon Quantum Dots and Photocatalyst Design. *Angew. Chem., Int. Ed.* **2010**, *49*, 4430–4434.

38. Zhang, N.; Dai, D.; Zhang, W.; Fan, J. Photoluminescence and Light Reabsorption in SiC Quantum Dots Embedded in Binary-Polyelectrolyte Solid Matrix. *J. Appl. Phys.* **2012**, *112*, 094315-1–094315-4.
39. Zheng, H.; Wang, Q.; Long, Y.; Zhang, H.; Huang, X.; Zhu, R. Enhancing the Luminescence of Carbon Dots with a Reduction Pathway. *Chem. Commun.* **2011**, *47*, 10650–10652.
40. Lai, L.; Potts, J. R.; Zhan, D.; Wang, L.; Poh, C. K.; Tang, C.; Gong, H.; Shen, Z.; Lin, J.; Ruoff, R. S. Exploration of the Active Center Structure of Nitrogen-Doped Graphene-Based Catalysts for Oxygen Reduction Reaction. *Energy Environ. Sci.* **2012**, *5*, 7936–7942.
41. Wang, P.; Wang, Z.; Jia, L.; Xiao, Z. Origin of the Catalytic Activity of Graphite Nitride for the Electrochemical Reduction of Oxygen: Geometric Factors *vs.* Electronic Factors. *Phys. Chem. Chem. Phys.* **2009**, *11*, 2730–2740.